Construction and testing of a Top Counting Detector and a Bottom Counting Detector for the Cosmic Ray Energetics And Mass experiment on the International Space Station

2015 JINST 10 P07018

(http://iopscience.iop.org/1748-0221/10/07/P07018)

PUBLISHED BY IOP PUBLISHING FOR SISSA MEDIALAB
RECEIVED: *March 2, 2015*
REVISED: *May 8, 2015*
ACCEPTED: *June 8, 2015*
PUBLISHED: *July 28, 2015*

Construction and testing of a Top Counting Detector and a Bottom Counting Detector for the Cosmic Ray Energetics And Mass experiment on the International Space Station

Y.S. Hwang,[a] H.J. Kim,[a,1] T. Anderson,[b] D. Angelaszek,[c] M. Copley,[c] S. Coutu,[b] J.H. Han,[c] H.G. Huh,[c] D.H. Kah,[a] K.C. Kim,[c] K. Kwashnak,[c] M.H. Lee,[c] J.T. Link,[d,e] L. Lutz,[c] A. Malinin,[c] J.W. Mitchell,[d] S. Nutter,[f] O. Ofoha,[c] H.B. Jeon,[a] H.J. Hyun,[a] H. Park,[a] J.M. Park,[a] P. Patterson,[c] E.S. Seo,[c] J. Wu[c] and Y.S. Yoon[c]

[a] *Kyungpook National University, Daegu 702-701, South Korea*
[b] *Pennsylvania State University, University Park, PA 16802, U.S.A.*
[c] *University of Maryland, College Park, MD 20742, U.S.A.*
[d] *NASA GSFC, Greenbelt, MD 20771, U.S.A.*
[e] *CRESST (USRA), Columbia, MD 21044, U.S.A.*
[f] *Northern Kentucky University, Highland Heights, KY 41076, U.S.A.*

E-mail: hongjoo@knu.ac.kr

ABSTRACT: The Cosmic Ray Energetics And Mass (CREAM) mission is planned for launch in 2015 to the International Space Station (ISS) to research high-energy cosmic rays. Its aim is to understand the acceleration and propagation mechanism of high-energy cosmic rays by measuring their compositions. The Top Counting Detector and Bottom Counting Detector (T/BCD) were built to discriminate electrons from protons by using the difference in cascade shapes between electromagnetic and hadronic showers. The T/BCD provides a redundant instrument trigger in flight as well as a low-energy calibration trigger for ground testing. Each detector consists of a plastic scintillator and two-dimensional silicon photodiode array with readout electronics. The TCD is located between the carbon target and the calorimeter, and the BCD is located below the calorimeter. In this paper, we present the design, assembly, and performance of the T/BCD.

KEYWORDS: Space instrumentation; Particle detectors

[1] Corresponding author.

doi:10.1088/1748-0221/10/07/P07018

2015 JINST 10 P07018

Contents

1 Introduction of the ISS-CREAM

Cosmic rays were discovered in 1912 by Hess [1]. The origin, acceleration, and propagation mechanism of cosmic rays remain unexplained. The energy spectrum of high-energy cosmic rays ($E > 10^5$ eV) has been measured directly and indirectly using various techniques [2, 3]. The energy of cosmic rays extends up past 10^{20} eV with the flux decreases rapidly following a power law as the energy increases. High-energy spectra from 10^5 eV to 10^{14} eV are assumed to be dominated by supernova shocks. The "knee" is a transition region where the energy spectrum of cosmic rays steepens from 10^{14} eV to above 10^{16} eV [4]. This region might be related to the supernova acceleration limit and might be connected with the origin of cosmic rays in supernova blast waves [5]. Therefore, it is important to observe the detailed energy dependence of all components around the "knee" to understand the origin, acceleration, and propagation mechanism of high-energy cosmic rays.

The balloon-borne Cosmic Ray Energetics and Mass (CREAM) experiment measured the composition of cosmic rays over an energy range of 10^{10} to 10^{14} eV on six flights that recorded a total exposure time of $\sim$ 161 days [6, 7]. The CREAM experiment on the International Space Station (ISS) is modified version of the CREAM balloon experiment which will increase our understanding of the "knee" in the cosmic rays energy spectrum. ISS-CREAM experiment will have a longer exposure time to cosmic rays and more stable experimental conditions than the balloon-borne experiments, reducing the statistical uncertainty significantly in high-energy cosmic rays studies. In addition, ISS-CREAM will be equipped with two new detector suites to investigate recent result showing an electron excess at $\sim 6 \times 10^{11}$ eV which might be evidence of dark matter annihilation or nearby unknown point sources [8, 9].

2015 JINST 10 P07018

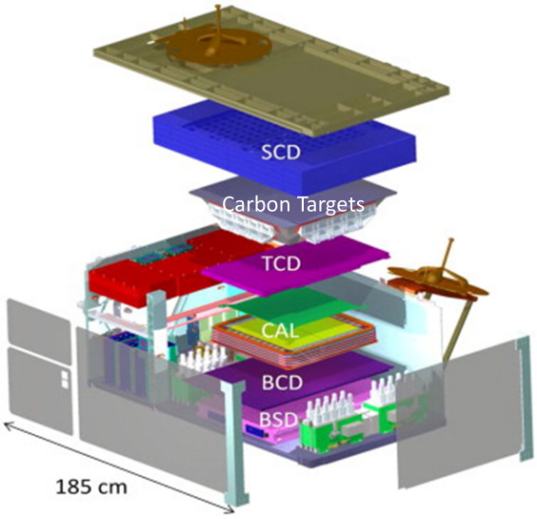

Figure 1. Schematic view of the ISS-CREAM instrument.

2 Overview of the ISS-CREAM instruments

Figure 1 shows the ISS-CREAM instrument which consists of four detector suites: the Silicon Charge Detector (SCD), the Calorimeter (CAL), the Top and Bottom Counting Detector (T/BCD) and the Boronated Scintillation Detector (BSD) [10].

The SCD precisely measures the charge of particles from atomic numbers of $Z = 1$ (H) to 28 (Ni). Electron-hole pairs are generated in the fully depleted silicon Positive-Intrinsic-Negative (PIN) diodes of the SCD when through-going particles lose their energy in the silicon PIN diodes [11]. These electron-hole pairs serve as the signal. The SCD consists of four layers each layer has 2688 ($1.5 \times 1.6\,\mathrm{cm}^2$) silicon PIN diodes to provide better charge resolution and tracking capability.

The CAL measures the energy from about 10^{11} eV to over 10^{15} eV. The CAL is a stack of twenty 3.5 mm thick ($1X_0$) tungsten plates of dimensions $50 \times 50\,\mathrm{cm}^2$ interleaved with layers of scintillating-fiber ribbons [12]. Each layer contains 50 ribbons and each $1 \times 50\,\mathrm{cm}^2$ ribbon has 19 muti-clad scintillating fibers of 0.5 mm diameter. The scintillating-fiber ribbons are excited by the shower of secondary particles induced in the carbon targets, with 19 cm of target material in total in the targets (for a $50 \sim 60\%$ probability of interaction of incident nuclei). Each tungsten plate has a short radiation length of $6.76\,\mathrm{g/cm}^2$ which provides a thin calorimeter stack. The thin calorimeter provides a large acceptance to increase detection efficiency, especially important because of low cosmic ray incidence rates. The scintillation light from the ribbons is read out by Hybrid Photo Diodes (HPD). The CAL also provides high-energy triggers to all the instruments via trigger boards [13].

The T/BCD provides shower profiles for electron/proton separation, a redundant energy trigger, and a Minimum Ionizing Particle (MIP) trigger for calibration of the other detectors in ground tests and is discussed in detail in the following sections.

The BSD is a boronated scintillation detector read out by $1''$ PMTs [14]. The BSD is designed to detect neutrons generated in the particle shower from particles interacting in the calorimeter.

2015 JINST 10 P07018

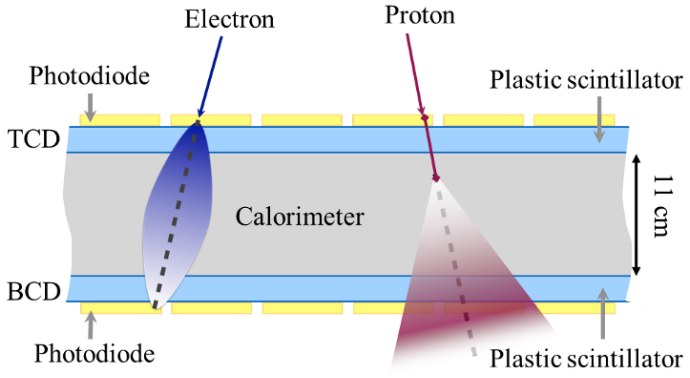

Figure 2. Shapes of showers caused by electromagnetic and hadronic interactions in the T/BCD.

The number of neutrons in the showers differs between electrons and hadrons at the same energy allowing the BSD to provide discrimination between the electrons and protons. This technique is independent from the discrimination technique used by the T/BCD allowing both measurements to be used together in a complimentary fashion.

3 The Top Counting Detector and Bottom Counting Detector

3.1 Introduction

Electrons and protons are separated in the T/BCD by measuring the number of hits from the two-dimensional PhotoDiode (PD) arrays. Hadronic shower is dominated by inelastic hadronic interactions. The physical processes that cause the propagation of the hadronic shower are considerably different from the electromagnetic showers. A typical hadronic shower is produced with bigger transverse momentum so that hadronic showers tend to be more laterally spread out than electromagnetic showers [15]. Thus it takes much longer to develop and goes much deeper than electromagnetic showers, as shown in figure 2. The TCD detects the particles back-scattered by hadronic interactions with the tungsten layers of the calorimeter. Also the T/BCD provides a trigger system for redundancy of the instruments and the energy calibration. The T/BCD trigger algorithm has two modes available. A high-energy mode is used to provide high energy trigger in cases when the calorimeter trigger is not working, and a low-energy mode is used for energy calibration of the other detectors by providing a muon trigger.

3.2 Design and assembly

In order to survive launch and operate in the vacuum of space the T/BCD instruments must be built to developed National Aeronautics and Space Administration (NASA) instrumentation standards. Requirements are levied on the type of materials that can be used to ensure they will not degrade nor outgas in the vacuum of space [16]. Additional requirements are levied on the electronics to ensure they can survive the radiation environment present in space. The instruments must be shown both by analysis and testing to survive the stresses and rigors of the acceleration and vibration environment encountered during a rocket launch. They also must be tested in a thermal-vacuum chamber to demonstrate their proper operation in the space environment.

2015 JINST 10 P07018

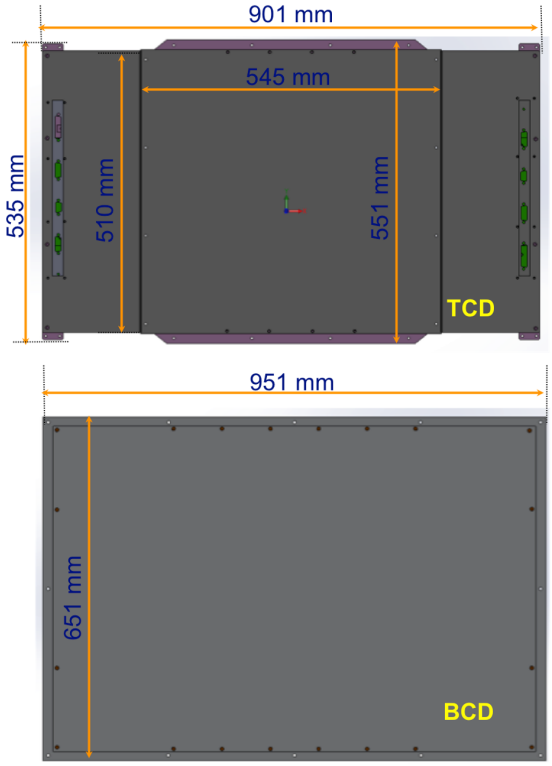

Figure 3. Dimensions and enclosures shape of the TCD (top) and the BCD (bottom).

Various frequency, acceleration, and temperature conditions are considered using the SolidWorks analysis software [17] to verify solidity of the T/BCD mechanical design. The T/BCD enclosures are fabricated from a 6061 aluminum alloy [18]. It is lighter and stronger than steel and that is widely used in the aerospace industry. The enclosure was chemically coated to prevent corrosion and increase the electrical resistance by following the MIL-A8625 standard [19]. The dimensions of the enclosures are $901 \times 551 \times 30\,\mathrm{mm}^3$ and $951 \times 651 \times 33\,\mathrm{mm}^3$, respectively, as shown in figure 3. The active detection areas in the T/BCD are $500 \times 500\,\mathrm{mm}^2$ and $600 \times 600\,\mathrm{mm}^2$, respectively. The masses of the T/BCD allocated to the payload were 13 kg and 16 kg, respectively. The assembled masses of the T/BCD are 9.6 and 15.6 kg, respectively, which satisfy the allocated mass for each detector.

Each detector consists of six Printed Circuit Boards (PCB) with PDs and electronics parts. The electronics are located at the outer sides of the detector. The PDs and scintillator are integrated in the middle of the detector, as shown in figure 4. The PCBs, 370HR (Isola Group) were fabricated to the IPC-CLASS 3/A standards, the typical quality acceptability requirement for aerospace environments [20]. The electrical components were soldered with solder paste consisting of Sn63:Pb37. Whole wires are connected with each board and port by using the "flying wiring" method. The signal lines use 24 gauge wire twisted-pairs to reduce the noise. The power lines use 20 gauge wire to meet current rating requirements. The PCBs, except for the PD areas, were conformal coated with CONATHANE CE-1150 (Cytec). A 1 mm-thick conformal coating was applied to stake the electronics parts and wires. The coating provides to prevent tin whiskering in space environments [21]

2015 JINST 10 P07018

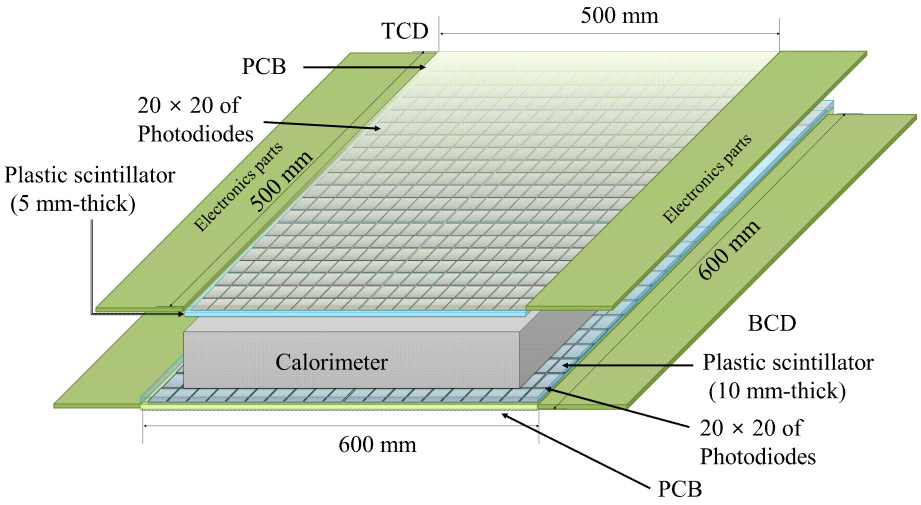

Figure 4. Design concept of the T/BCD.

and outstanding resistance to moisture, abrasion, and discharge in high-voltage circuits under low vacuum condition.

There are 400 PDs in a 20×20 array in each of the TCD and BCD. The dimensions of each PD are $23 \times 23 \times 0.65\,\mathrm{mm}^3$. The PD has an active area of $20 \times 20\,\mathrm{mm}^2$ and a light entrance window, and was designed and fabricated using standard photolithography techniques [22]. The leakage current was measured with a Keithley 6517A picoammeter, and the capacitance was measured with a HP4277A LCZ meter. The PDs are fully depleted well below $-200\,\mathrm{V}$. The leakage current of each PD was measured to be about $20\,\mathrm{nA/cm}^2$ at the operating voltage [23]. The radiation hardness of the PD was tested by using a 45 MeV proton beam at the Korea Institute of Radiological and Medical Sciences (KIRAMS). The PD sensor was exposed to approximately 10^{11} protons/cm^2, which corresponds to > 5000 rad/year. The leakage current was increased up to about $50\,\mathrm{nA/cm}^2$ but the quality of the PD sensor was not degraded [24].

The PD arrays were attached to a EJ-200, polyvinyl toluene plastic scintillator (Eljen Technology) with an emission wavelength of $400 \sim 500\,\mathrm{nm}$ [25]. The quantum efficiency at the emission wavelengths of the scintillator was measured to be $60 \sim 75\%$ [26].

Figure 5 shows how the PDs were aligned and fixed using an aluminum jig structure. A Eccobond 56 C, conductive epoxy (Hysol) was used to fix the PDs and form electrical connections between the PDs and the PCB.

The n-side of the PDs was connected to ground using a Polyimide Film cable and conductive epoxy. The plastic scintillators were attached to the PDs using of DC93-500 optical silicone adhesive (Dow Corning), as shown in figure 6. Vacuum was applied to remove entrapped air during mixing optical silicone adhesive for 20 min at 10^{-3} Torr. The dimensions of the plastic scintillators for the T/BCDs were $500 \times 500 \times 5\,\mathrm{mm}^3$ and $600 \times 600 \times 10\,\mathrm{mm}^3$, respectively. Each plastic scintillator was divided into six pieces of the same size as the sensor parts of the PCBs.

The plastic scintillators were wrapped in Enhanced Specular Reflector (ESR) light reflector (3M Vikuiti) for increasing light collection efficiency (figure 7). The light reflector has a very thin thickness (0.065 mm) and high reflectance ($> 98\%$). The reflector was heat formed around

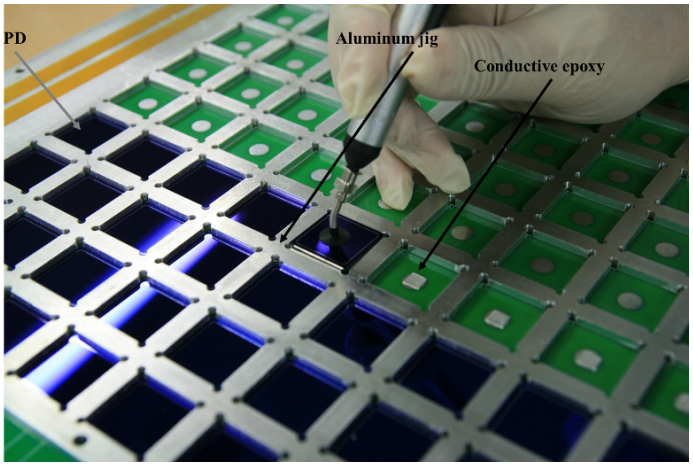

Figure 5. The assembly of the PDs with the conductive epoxy by using the aluminum jig structure.

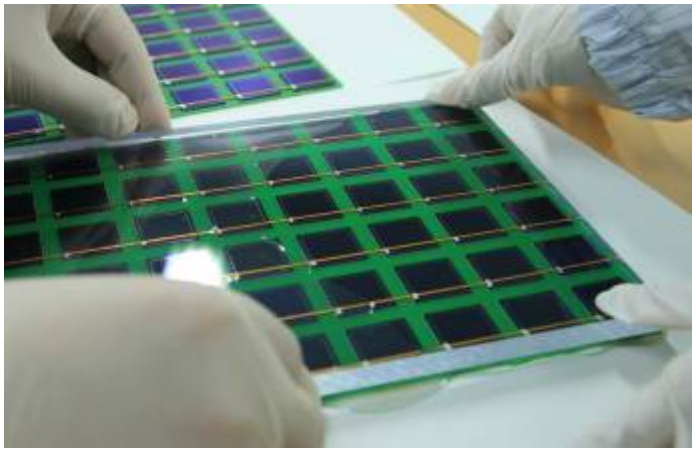

Figure 6. Coupling of the plastic scintillator and the PDs by using the optical silicone adhesive.

the scintillator using a custom aluminium mold by heating the reflector to 60°C for 12 hours. A Polyimide Film Tape 92 (3M) was used form a light seal around the shaped light reflector and the plastic scintillator.

A sheet of Poron Foam (Rogers corporation) 0.9 mm-thick was placed on the top and bottom sides of the detector (figure 8) to prevent damage due to vibration and to absorb shock. Finally all connectors were assembled to the enclosures.

3.3 Readout electronics

The electronics systems of the TCD and BCD are each composed of two mother boards and four daughter boards, as shown in figure 9. Each mother board consists of three Application-Specific Integrated Circuit (ASIC) chips, one Field-Programmable Gate Array (FPGA) chip, and two high-voltage circuits for biasing the PDs. The mother boards serve to data collection of all ASIC chips, control signal for all active chips and power for all PDs. Each daughter board holds just two ASIC chips for data collection of 60 PD's data. We selected VA32HDR14.2 (VA) and TA32CG3 (TA) for

2015 JINST 10 P07018

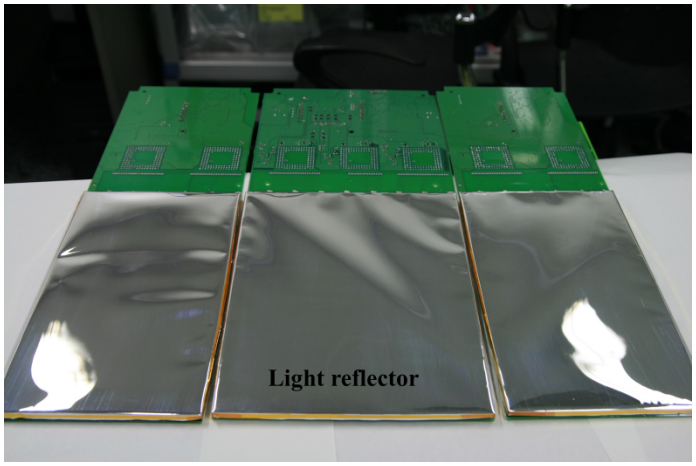

Figure 7. The light reflector material was wrapped around one set of the BCD plastic scintillator.

Figure 8. Final assembly of the detectors and connectors without a cover.

our ASIC chips to mitigate radiation hardness and high dynamic range and a A3P250 (MicroSemi) for our FPGA to mitigate radiation hardness [27, 28]. All of these chips were tested using a heavy ion beam to ensure they could survive the space radiation environments [29, 30].

The signals from the PDs are sent to the 32 channels of charge-sensitive fast preamplifier and slow shaper of the VA. The preamplifier signals are compared with the threshold voltages by the level-sensitive discriminator in the TA. The threshold voltages are externally adjustable using a digital-to-analog converter. The TA generates an OR'ed trigger signal from the inputs of all 32

2015 JINST 10 P07018

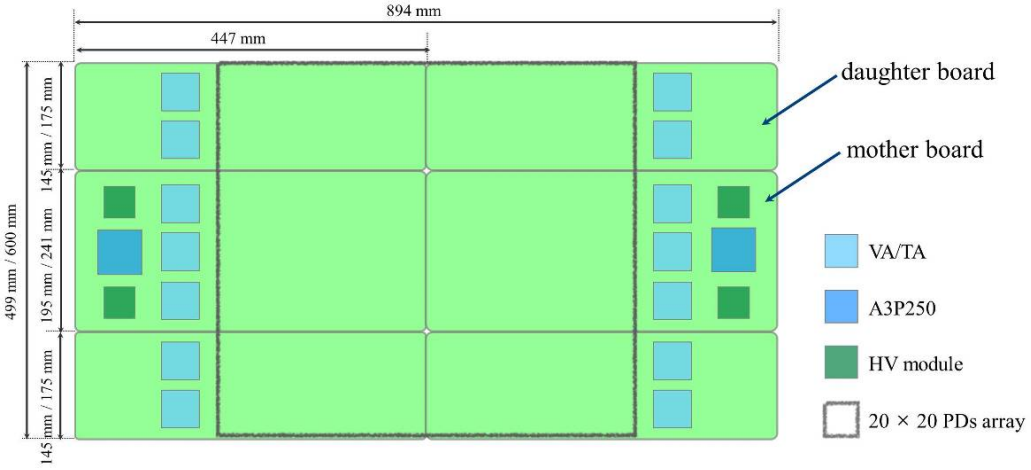

Figure 9. The T/BCD electronics system.

channels. The valid triggered signals received from the trigger board to drive the hold circuit. The hold circuit of the VA maintains the signal of the slow shaper. Then holding voltage signals are provided by an external clock source. The analog signals are then digitized by a 16-bit-resolution analog-to-digital converter (AD7663, Analog Devices). The input range of the AD7663 is -2.5 V to $+2.5$ V. One least significant bit is 76.3 μV.

A Q12-03, High Voltage (HV) module (EMCO) supplies a bias to the PDs. The input and output voltages of the HV module are $+12$ V and -210 V, respectively. One HV module can be supply 200 of the PDs with 4 mW.

Various control logics for power on/off, threshold control, VA/TA operation and high voltage on/off was developed and included to the A3P250 chips.

The measured total power of the T/BCD is about 22 W at the idle state, less than the budgeted total power of 40 W.

4 Environmental tests

A thermal-vacuum test was performed at a pressure of 1×10^{-5} Torr to verify the operation and survival of the detectors. While under vacuum, the temperature was cycled between -40°C and $+55$°C to simulate the worse case and between -20°C and $+40$°C to simulated the operation case in space environments. A vibration test was also performed to qualify the survival of the T/BCD in the worse case of launch and ascent conditions. These tests verify the mechanical design and workmanship of the T/BCD.

During the thermal-vacuum test we experienced two issues. The first was the power drop at the low temperature. The basic currents circuit is designed to fit two VA/TA chips. The mother boards have three ASIC chips that consumed more power. Thus we increase the current limiter value by three ASIC chips. The Second was the conversion signal has double edge it make wrong reset signal. We attached the 33 pC capacitor from conversion signal to ground to make broad shape.

There were no issues with the vibration test, a visual inspection verified no damage or loosened components and there was no change in fundamental frequency response after the test. The T/BD

2015 JINST 10 P07018

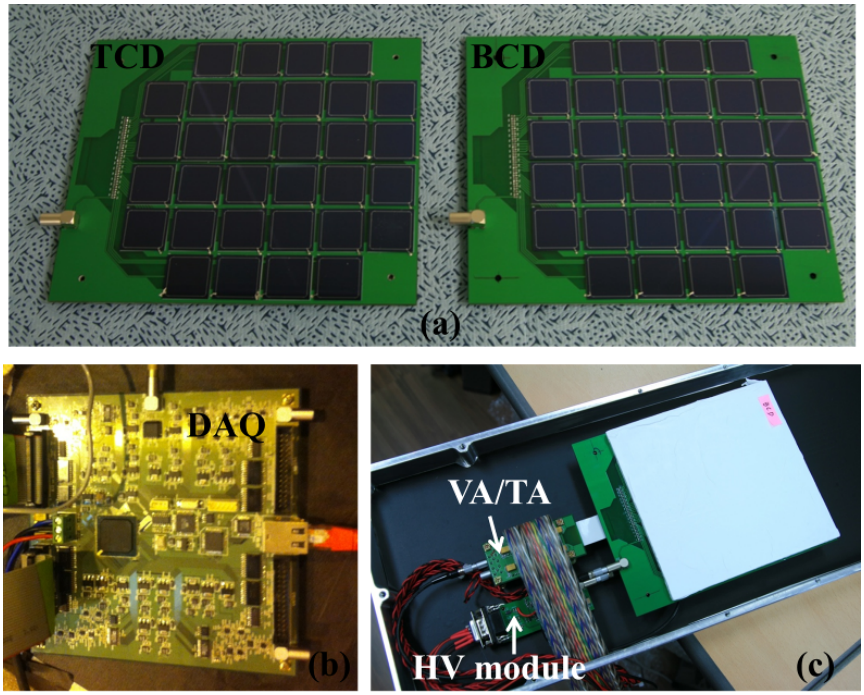

Figure 10. (a) Prototype T/BCD modules each with 32 PDs. (b) DAQ system with commercial board. (c) VA/TA module and HV module coupled with the BCD.

was also functionally tested after this test and worked without issue. The T/BCD was delivered to NASA Wallops Flight Facility (WFF) in April 2014 for integration and instrument level testing which is currently on going.

5 CERN beam test

A prototype T/BCD each with 32 PDs was tested at the H2A CMS test beam facility in the European Organization for Nuclear Research (CERN) to check the capabilities of electron/proton separation and MIP trigger. The upper (a), lower left (b), and lower right (c) photos in figure 10 show the prototype modules, Data AcQuisition (DAQ) electronics with the Xilinx FPGA, and readout electronics with the 128 channels VA/TA board, respectively. We check possibility of electron and proton separation with PDs which was developed in the KNU since we used the commercial DAQ electronics and readout electronics.

The experimental setups are shown in figure 11(a) and (b). The prototype T/BCD modules were placed at the bottom of the entire setup as shown in figure 11(a) to measure the MIP signals. Figure 11(b) is to compare the hit distribution of the TCD and BCD for different beam source such as electrons and pions. In this setup the CAL module provides the trigger signal to the prototype T/BCD modules.

The 150 GeV electron beam includes muons and the MIP is measured by using these punch through muons. As shown in figure 12, the MIP signal was measured to be 2454 ADC. The measured mean and standard deviation of the pedestal distribution were 2092 ADC and 46 ADC,

2015 JINST 10 P07018

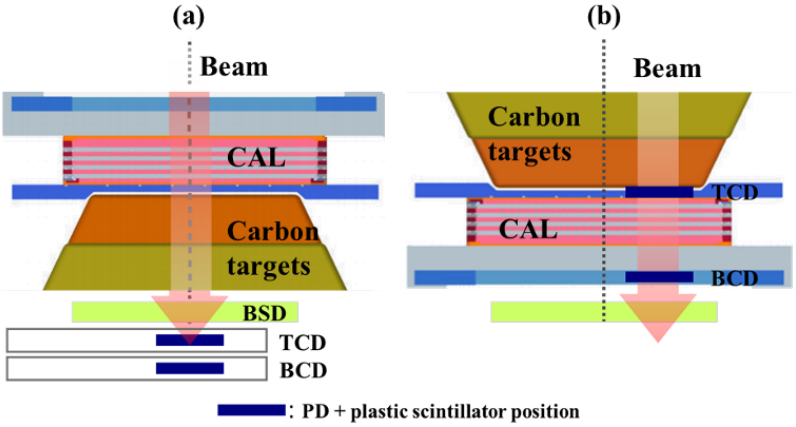

Figure 11. Diagram of the experimental setup. (a) MIP measurements configuration. (b) Hit distribution measurements configuration to compare electron and pion beams.

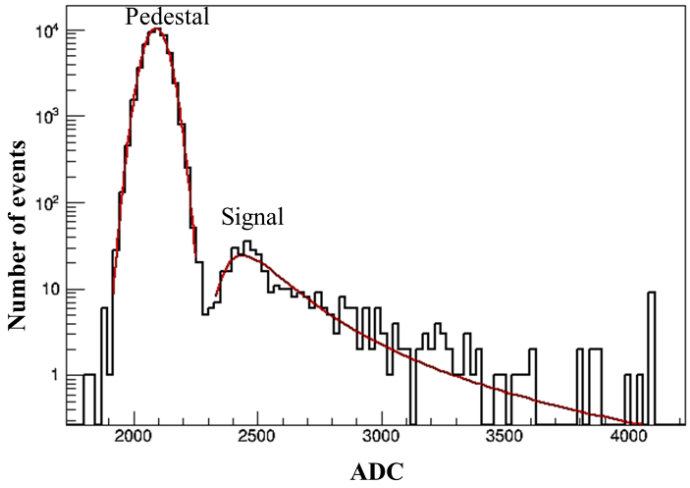

Figure 12. The SNR of 7.9 was measured with the prototype module by using an electron beam.

respectively. We obtained a Signal-to-Noise Ratio (SNR) of 7.9, which satisfies the detector's design performance requirement of SNR > 5.

Figure 13 shows the different response areas of the prototype BCD between a electron (a) and a pion (b) beam using high energy threshold. We compared a 75 GeV electron and a 250 GeV pion beam since the pion has π^+, π^- and π^0 mode. Thus we choose the 250 GeV energy of pion beam which is three times bigger than the 75 GeV energy of electron beam. The response areas which interact with a pion beam are wider than an electron beam. These results indicate the capability of separation between electron and proton by using shower shapes in the T/BCD.

The fraction of energy deposited via electromagnetic cascades in hadronic showers varies widely [31–33]. We use shower shape variables similar to the ones developed for the electron and proton separation in the ATIC analyses [34]. A GEANT3 Monte Carlo simulation package [35] was used to separate electromagnetic cascades from hadronic showers over a wide energy range, which will be described in another paper under development.

2015 JINST 10 P07018

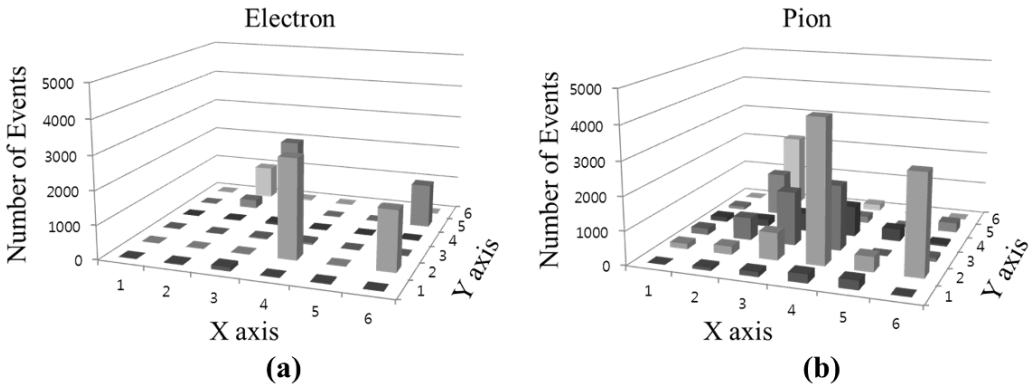

Figure 13. The different response areas between (a) 75 GeV electron and (b) 250 GeV pion beams in the prototype BCD.

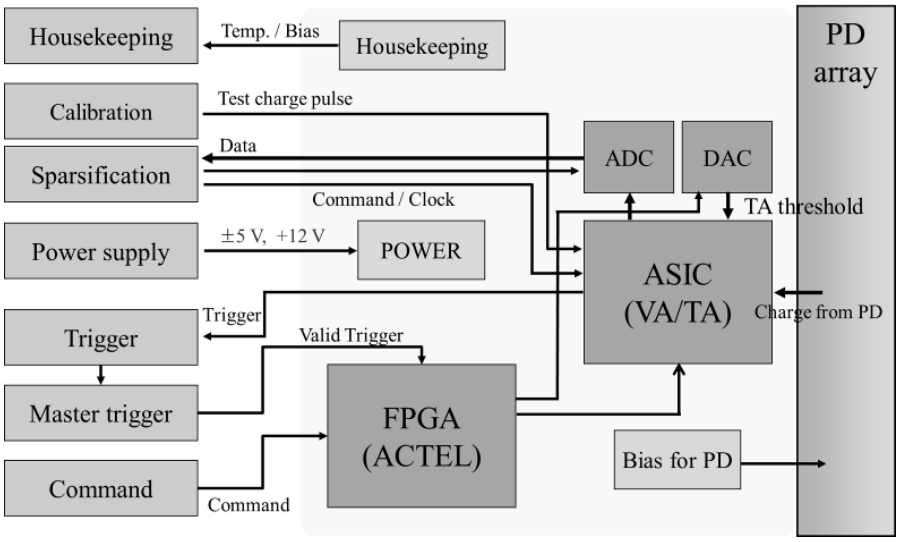

Figure 14. Diagram of the readout electronics system for the T/BCD.

6 Performance of the T/BCD

Figure 14 shows how the T/BCD readout electronics connects with the balloon-borne CREAM electronics. We prepare the T/BCD detector earlier then ISS-CREAM common electronics. But those systems have same functions with ISS-CREAM common electronics since it can be probe the performance of the T/BCD electronics. The common electronics system for testing the T/BCD consists of electronics to provide sparsification, trigger, master trigger, calibration, command, and housekeeping functions. The sparsification board collects the ASIC data from the PDs. The trigger board collects the trigger signals from the T/BCD and sends the trigger information to the master trigger board by selecting the trigger logic. The master trigger board records the address of each trigger board and provides effective trigger signals to all detectors. The calibration board provides a known charge to each of the 896 channels to analyze their responses as well as a test pulse for triggering. The housekeeping module collects all the detector's current, voltage, and temperature

2015 JINST 10 P07018

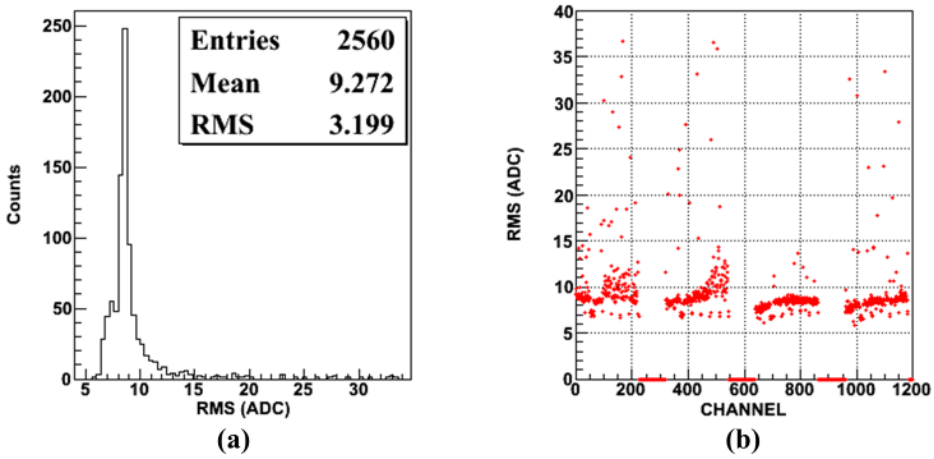

Figure 15. Pedestal distribution plot. (a) Distribution of the pedestal RMS for all channels. (b) RMS of each channel.

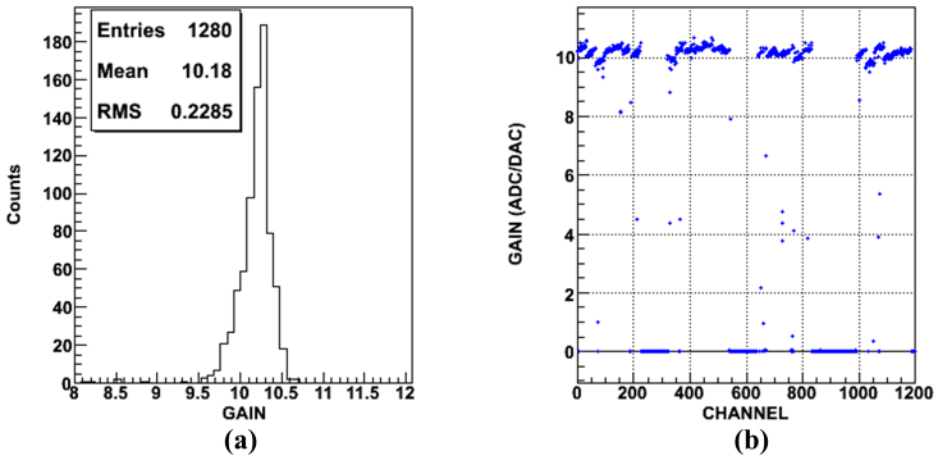

Figure 16. Single charge test result. (a) Distribution of the gain for all channels. (b) Gain of each channels.

information to ensure the safety of all systems. The T/BCD provide the bias voltage monitoring value and temperature of each motherboard.

We have made noise, calibration, and muon tests are needed to confirm the MIP trigger performance. The pedestal and calibration data are used to calculate the SNR by comparing the muon data for the low-threshold trigger capability with that of proper level setting. Figure 15(a) shows the pedestal RMS distribution for all channels which mean of all channels pedestal RMS is about 9.27 ADC and (b) shows the pedestal RMS values of the each channel which is enough to measure the muon signal.

Figure 16(a) shows the gain distribution of the all channels which mean value is 10.2 ADC/DAC and (b) is the gain values of the each channel. An input test pulse of 2000 DAC (about 300 mV) was applied to a test charge of 3 pC through a 10 pF coupling capacitor for the charge calibration. One ADC corresponds to about 900 electrons since the conversion gain is 7 ADC/fC. Thus, 8200 noise electrons is equivalent to 0.7 mV at the VA.

2015 JINST 10 P07018

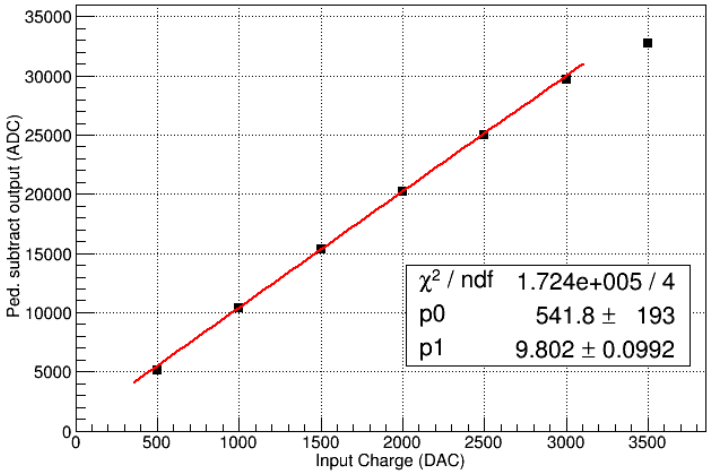

Figure 17. Charge inputs versus outputs ADC for measuring the linearity of the VA.

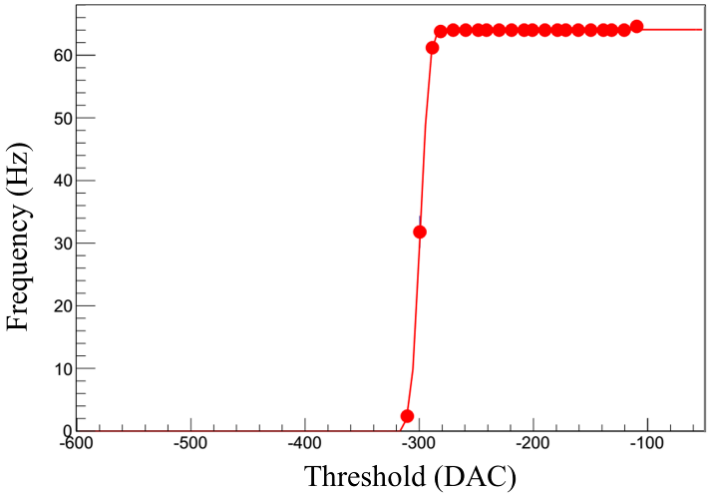

Figure 18. Trigger rate increase from −300 DAC. The trigger noise value is about 6.54 DAC.

From the 161 days of accumulated flight exposure in 6 balloon flights, we have learned that the changes in pedestal RMS noise with respect to temperature variation from about 0°C to 30°C were negligible comspared to the noise itself. For ISS-CREAM, we expect a similar range of temperature variations and thus a similar performance of the readout electronics.

Figure 17 shows linearity and the dynamic range of one channel of the VA. The VA has good linearity with input charge from 700 fC to 4.5 pC. The channel was saturated at 3500 DAC, corresponding to 5.2 pC.

The trigger gain run measured the rate of the TA trigger signals when a test charge applied with various threshold values as shown in figure 18. When a 100 fC input charge is applied to the VA chip, the TA sends trigger signals starting at about −300 DAC. As a result, the trigger gain is 3 DAC/fC. A trigger noise value is about 6.54 DAC. The data is fitted using a Gaussian convoluted step function.

2015 JINST 10 P07018

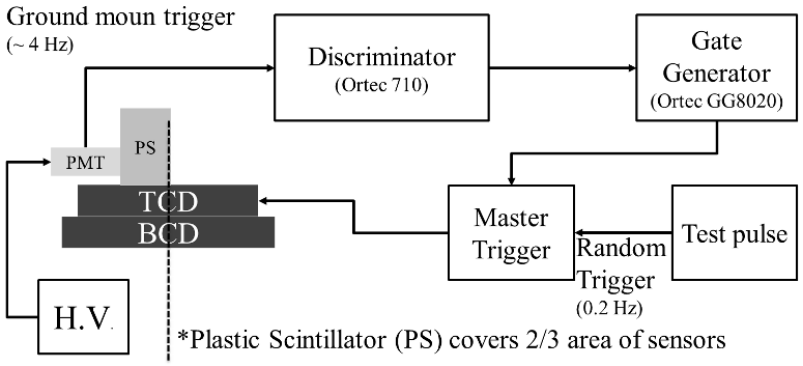

Figure 19. Diagram for the muon response test of the T/BCDs using an external trigger system.

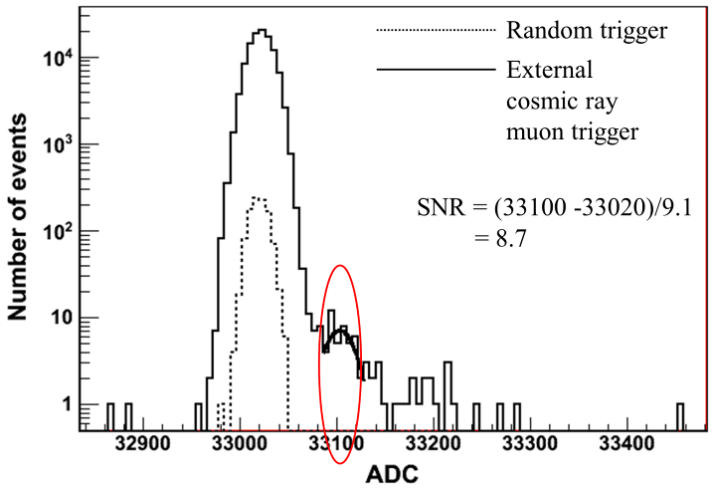

Figure 20. Cosmic rays muon experimental data. Dotted line is pedestal spectrum, which mean value is 33,020 ADC. Solid line is muon signal, which mean value is 33,100 ADC.

Figure 19 is a diagram for the muon response test experimental setup. The $12 \times 80\,\mathrm{cm}^2$ ($960\,\mathrm{cm}^2$) plastic scintillator attached to a 2 inch PhotoMultiplier Tube (PMT), and was used to trigger system of cosmic rays muon. These signals were then converted to trigger signals using a gate generator. The trigger signals are applied to the master trigger board. The master trigger board sent the trigger signals to the T/BCD. The test result is shown in figure 20. The solid line shows the signal data, which was triggered by the PMT in one channel of the TCD. The dotted line is the pedestal distribution in the same channel. The muon signal appeared around 33,100 ADC. The peak value of the subtracted background was 80 ADC, which corresponds to 11.4 fC (71,250 electrons). Since T/BCD consists of plastic scintillator coupled with PD, the light of plastic scintillator increase the total muon signal. Thus the expected muon signal of T/BCD is about ~ 9.2 fC. The measured value is higher than the expected muon value since we use only one trigger system and measure higher signals. The result shows that the T/BCD can measure the MIP signals for the calibration. The calculated SNR with the above result is 8.7 and it satisfies the requirement of SNR > 5.

2015 JINST 10 P07018

7 Summary

The T/BCD for the CREAM mission, which is planned to launch to the ISS in 2015, has successfully been built and delivered to WFF for integration. The T/BCD has been designed and developed to separate electrons from protons. For this purpose, the experiment requires space-grade quality in all of the detectors, materials, and functions. Both detectors consist of plastic scintillators, PDs, and readout electronics. The dimensions of arrays of 400 PDs attached to the plastic scintillators of the T/BCD are $500 \times 500\,\mathrm{mm}^2$ and $600 \times 600\,\mathrm{mm}^2$, respectively. The estimated masses of the T/BCD are 9.6 and 15.6 kg, respectively, which satisfy the mass limitations. The power consumption of the detectors is 22 W, which is less than the allocated power (40 W). The T/BCD passed environmental tests such as thermal, vacuum, and vibration tests. To achieve the scientific goals, the readout electronics provide the electron/proton shower profile, the redundant trigger, and the MIP trigger. In the tests including noise, gain, trigger, and cosmic ray tests, all the functions were performed normally with balloon-borne CREAM common electronics. The T/BCD is now testing with the ISS-CREAM common electronics in the WFF. And T/BCD will undergo final environment tests in the United States after total integration.

Acknowledgments

That was supported by National Research Foundation (NRF) of Korea grants funded by the Korean Government (NRF-2011-0016260). The authors thank NASA Goddard Space Flight Center (GSFC) Wallops Flight Facility for project management and engineering support, and NASA Johnson Space Center ISS Program Office for launch support and ISS accommodations. This work was supported in the United States by NASA grants NNX11AC52G, NNX08AC15G, and NNX08AC16G and their predecessor grants, as well as by directed RTOP funds to the NASA GSFC. It was partially funded by the project titled "Research on fundamental core technology for ubiquitous shipping and logistics" funded by Ministry of Oceans and Fisheries, Korea.

References

[1] V.F. Hess, *Über Beobachtungen der durchdringenden Strahlung bei sieben Freiballonfahrten*, *Phys. Zeit.* **13** (1912) 1084.

[2] E.S. Seo, *Direct measurements of cosmic rays using balloon borne experiments*, *Astropart. Phys.* **39-40** (2012) 76.

[3] M. Nagano and A. Alan, *Observations and implications of the ultrahigh-energy cosmic rays*, *Rev. Mod. Phys.* **72** (2000) 689.

[4] M. Amenomori et al., *The cosmic-ray energy spectrum between* $10^{14.5}$ *and* $10^{16.3}$ *eV covering the"knee" region*, *Astrophys. J.* **461** (1996) 408.

[5] P.O. Lagage and C.J. Cesarsky, *The maximum energy of cosmic rays accelerated by supernova shocks*, *Astron. Astrophys.* **125** (1983) 249.

[6] E.S. Seo et al., *Cosmic-Ray Energetics And Mass (CREAM) balloon project*, *Adv. Space Res.* **33** (2004) 1777.

2015 JINST 10 P07018

[7] H.S. Ahn et al., *Measurements of the relative abundances of high-energy cosmic-ray nuclei in the TeV/nucleon region*, *Astrophys. J.* **715** (2010) 1400.

[8] J. Chang et al., *An excess of cosmic ray electrons at energies of 300–800 GeV*, *Nature* **456** (2008) 362.

[9] FERMI LAT collaboration, M. Ackermann et al., *Measurement of separate cosmic-ray electron and positron spectra with the Fermi Large Area Telescope*, *Phys. Rev. Lett.* **108** (2012) 011103 [arXiv:1109.0521].

[10] E.S. Seo et al., *Cosmic Ray Energetics And Mass for the International Space Station (ISS-CREAM)*, *Adv. Space Res.* **53** (2014) 1451.

[11] I.H. Park et al., *Silicon charge detector for the CREAM experiment*, *Nucl. Instrum. Meth.* **A 570** (2007) 286.

[12] H.S. Ahn et al., *Energy spectra of cosmic-ray nuclei at high energies*, *Astrophys. J.* **707** (2009) 593 [arXiv:0911.1889].

[13] H.S. Ahn et al., *The Cosmic Ray Energetics And Mass (CREAM) instrument*, *Nucl. Instrum. Meth.* **A 579** (2007) 1034.

[14] T. Anderson et al., *The ISS-CREAM boronated scintillator detector*, in Proceedings of the *33rd International Cosmic Ray Conference (ICRC2013)*, Rio de Janeiro Brazil, 2–9 Jul 2013, ID 0350.

[15] W.R. Leo, *Techniques for nuclear and particle physics experiments: a how-to approach*, Springer (1994), pg. 59.

[16] A.W. Campbell and J.J. Scialdone, *Outgassing data for selecting spacecraft materials*, NASA Reference Publication (1993), http://outgassing.nasa.gov.

[17] SolidWorks Corporation, *Introducing SolidWorks*, Concord U.S.A. (2002).

[18] R.J. Davis ed., *Properties and selection: nonferrous alloys and special-purpose materials*, ASM Handbook Volume 2, ASM International (1990).

[19] United States Department of Defense, *Military specification. Anodic coatings for aluminum and aluminum alloys*, MIL-A-8625E, Washington D.C. U.S.A. (1988).

[20] IPC, *Acceptability of electronic assemblies*, IPC-A-610E (2010), http://www.ipc.org.

[21] T.A. Woodrow, *Evaluation of conformal coatings as a Tin Whisker mitigation strategy*, http://calce.umd.edu/lead-free/tin-whiskers/WoodrowConfCoatPres.pdf.

[22] D.H. Kah et al., *Fabrication and performance test of a silicon photo-strip detector coupled with a crystal scintillator*, *Nucl. Instrum. Meth.* **A 628** (2011) 256.

[23] H.J. Hyun et al., *Development of top/bottom counting detectors for the CREAM experiment on the ISS*, in Proceedings of the *33rd International Cosmic Ray Conference (ICRC2013)*, Rio de Janeiro Brazil, 2–9 Jul 2013, ID 1017.

[24] J.B. Bae, H.J. Hyun, D.H. Kah, K.H. Kang and H.B. Park, *Electrical characteristics and radiation detection performance of large-area photodiodes*, *J. Korean Phys. Soc.* **63** (2013) 1418.

[25] C. Hurlbut, *Eljen technology*, Sweetwater U.S.A., private communication (2002), http://www.eljentechnology.com/index.php/products/plastic-scintillators/48-ej-200.

[26] Y.S. Hwang, *Development of top counting and bottom counting detector for ISS-CREAM experiment*, Thesis, Kyungpook National University (2014).

[27] IDEAS, *Specifications. Model VA32HDR14.2 and TA32CG3*, http://ideas.no.

2015 JINST 10 P07018

[28] Microsemi Co., *Datasheet. Model A3P250*, http://www.microsemi.com.

[29] Larry Lutz et al., *SEE test report. T041711_T062811_VA32HDR_TA32,* (2011), http://radhome.gsfc.nasa.gov.

[30] Y. Amare et al., *Study of radiation effects on CREAM electronics*, in Proceedings of the *33rd International Cosmic Ray Conference (ICRC2013)*, Rio de Janeiro Brazil, 2–9 Jul 2013, ID 0630.

[31] D.E. Groom, *Energy flow in a hadronic cascade: application to hadron calorimetry*, *Nucl. Instrum. Meth.* **A 572** (2007) 633 [*Erratum ibid.* **A 593** (2008) 638] [physics/0605164].

[32] O. Adriani et al., *PAMELA measurements of cosmic-ray proton and helium spectra*, *Science* **332** (2011) 69 [arXiv:1103.4055].

[33] AMS collaboration, M. Aguilar et al., *Precision measurement of the* $(e^+ + e^-)$ *flux in primary cosmic rays from 0.5 GeV to 1 TeV with the Alpha Magnetic Spectrometer on the International Space Station*, *Phys. Rev. Lett.* **113** (2014) 221102.

[34] J. Chang et al., *Resolving electrons from protons in ATIC*, *Adv. Space Res.* **42** (2008) 431.

[35] R. Brun, F. Carminati and S. Giani, *GEANT. Detector description and simulation tool*, CERN Program Library Long Writeup W5013.

2015 JINST 10 P07018